



Amorphous-quantized WO₃·H₂O films as novel flexible electrode for advanced electrochromic energy storage devices

Bon-Ryul Koo^a, Myeong-Hun Jo^b, Kue-Ho Kim^b, Hyo-Jin Ahn^{a,b,*}

^a Program of Materials Science & Engineering, Convergence Institute of Biomedical Engineering and Biomaterials, Seoul National University of Science and Technology, Seoul 01811, South Korea

^b Department of Materials Science and Engineering, Seoul National University of Science and Technology, Seoul 01811, South Korea

ARTICLE INFO

Keywords:

Electrochromic energy-storage devices
Flexible electrodes
WO₃·H₂O
Amorphous quantization
Low-temperature processing

ABSTRACT

The existing synthetic approaches for high-performance WO₃-based electrodes require energy-intensive instrumentation and complex processing, which hinder the development of flexible electrochromic (EC) energy storage devices. Herein, new low-temperature-synthesized amorphous (a)-quantized WO₃·H₂O films for application in EC energy storage devices are proposed. The WO₃·H₂O films are fabricated by the spontaneous hydrolysis of a spin-coated WCl₆ solution by the water molecules in the surrounding atmosphere followed by annealing at 80 °C. This is an original and unique concept in that the induced quantization of a-WO₃ increases the number of electroactive sites, provides abundant oxygen vacancies, and widens the band gap, while the intercalated water molecules stabilize the structure, resulting in efficient charge transfer and stress alleviation during electrochemical reactions. Consequently, the transmittance (53.8% at 633 nm) and specific capacitance (78.5 F g⁻¹ at 1 A g⁻¹) of the flexible electrodes improves. Additionally, the carrier concentration and mobility increase due to a-WO₃ quantization, thereby increasing the electrical conductivity, resulting in the rapid switchability (3.7 s for coloration and 2.9 s for bleaching) and high rate capability of the flexible electrodes. The flexible solid-state devices light a 1.5 V white-light-emitting diode and maintain their good EC energy storage performance (76.1% transmittance modulation and 73.1% specific capacitance) even after 300 bending cycles at a bending radius of 1.3 cm. Therefore, the proposed a-quantized WO₃·H₂O films are promising active electrodes for flexible EC energy storage devices.

1. Introduction

With increasing serious environmental pollution and the progressive depletion of non-renewable resources, the development of controllable devices for energy storage, conversion, and conservation, such as smart windows, electrochemical capacitors, lithium-ion batteries, and solar cells, has become a global priority [1-4]. Among these, smart windows, which can dynamically control sunlight and solar radiation entering a building owing to their various optical properties (e.g., transmittance, absorption, and color), are a promising candidate for ensuring the energy efficiency and indoor comfort of buildings and other structures. The light-modulating behavior originates from ion insertion/extraction and the transfer of electrons to electroactive material under an applied voltage. Such electrochromic (EC) materials have potential applications in optical displays and rear view mirrors [1]. Similar to pseudocapacitors, EC devices store energy via reversible redox reactions; hence, such

devices offer the attractive combination of electrochromism and energy storage, which can open new application possibilities such as multi-functional smart windows that can sense the level of stored energy and accordingly change the optical property [5,6]. In future, devices with shape-adjustable functions are required for application in flexible or wearable devices. Polymer based flexible substrates, such as polyethylene terephthalate, polyethylene naphthalate (PEN), and poly(methyl methacrylate) (PMMA) offer the advantages of low product weight and ease of adaptability or the replacement of glass substrates in other applications [7,8]. However, only a few studies have successfully produced flexible EC energy-storage devices, and much research work is required for the commercialization of these devices [1,9].

To achieve the smooth performance of flexible EC energy-storage devices, which have a sandwich-like configuration of transparent conducting film/anodic active film/electrolyte/cathodic active film/transparent conducting film, both the development of active materials with

* Corresponding author.

E-mail address: hjahn@seoultech.ac.kr (H.-J. Ahn).

<https://doi.org/10.1016/j.cej.2021.130383>

Received 10 February 2021; Received in revised form 10 May 2021; Accepted 13 May 2021

Available online 20 May 2021

1385-8947/© 2021 Elsevier B.V. All rights reserved.

outstanding EC and pseudocapacitive characteristics against repeated mechanical strain and their deposition on polymeric transparent conducting films are important [10–12]. The majority of the few studies on flexible EC energy-storage devices used conducting polymers, such as poly(3,4-ethylenedioxythiophene)–poly(styrene sulfonate) and polyaniline as active materials owing to their intrinsic ductility and high EC and capacitive characteristics [1,13]. In addition, WO_3 as a representative transition metal oxide has been used in flexible EC energy-storage devices. However, in these studies, WO_3 was combined with one-dimensional nanostructures (Ag nanowires and ZnO nanorods) to obtain nanocomposite film to enhance the mechanical properties and charge transport [14–16]. In these works, WO_3 was deposited by thermal evaporation or pulsed laser deposition, which are expensive methods involving multiple processing steps and requiring complex equipment, and are therefore unsuitable for large-scale and low-cost applications [9,17]. A somewhat more efficient method is the direct deposition of pre-synthesized nanoparticles on polymeric substrates as a film by solution-based deposition methods such as spin coating and inkjet coating, which have the advantages of low cost and simple processing and do not require high-temperature annealing. However, a limitation of this method is that the nanomaterial synthesis process needs to be optimized to obtain desired nanostructures (nanoflakes and nanosheets) being available against taken mechanical strain and the dispersion and adhesion of the nanomaterials on the substrates needs to be improved to achieve the best performance of the flexible devices [18–20]. Against this background, the direct fabrication of film nanostructures from precursors on polymeric substrates at low decomposition temperatures (150–170 °C for PET, 85–105 °C for PMMA) could be the simplest and most effective method for fabricating flexible devices. This method is beneficial for fabricating various film nanostructures (porous, dope, and composite) with outstanding electrochemical properties for application in high-performance EC devices and electrochemical capacitors by varying the type of precursors, solvents, and additives in the solution. However, unlike in the case of rigid substrates, which generally endure high temperatures, a suitably low annealing temperature (250–500 °C) is required for the hydrolysis or polymerization of the precursors to avoid the thermal deformation of polymeric substrates at high temperatures [1,21,22]. Therefore, the fabrication of high-performance WO_3 films by low-temperature processes, which has not been attempted so far, is a revolutionary research concept that can expand device functionality to achieve flexibility or elasticity in the future.

In this study, to realize the above expectations, we developed low-temperature-synthesized amorphous (a)-quantized $\text{WO}_3\cdot\text{H}_2\text{O}$ films. Compared to closest similar materials such as amorphous and crystalline WO_3 films, the novelty of a-quantized $\text{WO}_3\cdot\text{H}_2\text{O}$ films is a build-up of defective structure to be effective for performance improvement of flexible electrochromic energy-storage devices. As an expected defective impact, the frank disorder and stacking fault of WO_3 structure induced by intercalated H_2O molecules can relax structural stress and electrostatic repulsion to effectively reduce diffusion barriers or migration energy of protons and alkali ions during electrochemical reactions [23]. In addition, abundant oxygen vacancies formed by the amorphous quantization can lead to improvement of electron density accelerating electrical and electrochemical behavior [24]. The low-temperature synthesis involving annealing at 80 °C is an advanced process for fabricating WO_3 -based flexible electrodes on flexible polymeric substrates, which would expand their application scope. The $\text{WO}_3\cdot\text{H}_2\text{O}$ films are fabricated by the spontaneous hydrolysis of spin-coated WOCl_4 and the surrounding H_2O molecules. Such a-quantized $\text{WO}_3\cdot\text{H}_2\text{O}$ films have the advantages of both high electrochemical activity and kinetics, which are useful for their application in flexible EC energy-storage devices owing to the amorphization of the films induced by the unique energy-efficient approach. Because of the unique effects, the induced defects in the film structure increase the number of electroactive sites for Li insertion, and the change in electronic structure renders the electrodes more transparent and kinetically sensitive. In addition, the H_2O

molecules intercalated in the films play a major role in structure stabilization, resulting in efficient charge transfer and stress relaxation of the electrode during the electrochemical reactions. Thus, the a-quantized $\text{WO}_3\cdot\text{H}_2\text{O}$ films exhibit excellent EC energy-storage performances in the assembled devices along with together with mechanical flexibility.

2. Experimental section

The a-quantized $\text{WO}_3\cdot\text{H}_2\text{O}$ films were fabricated by the spontaneous hydrolysis of a spin-coated WOCl_6 solution by the surrounding H_2O molecules followed by low-temperature annealing at 80 °C. The WOCl_6 solution was prepared by dissolving WOCl_6 (10 wt%; Aldrich) in 2-propanol (Aldrich) with continuous stirring at fixed temperature of 0 °C for protecting unwanted reaction of precursor. The resulting transparent blue solution was spin-coated twice on FTO (Pilkington, 8.0 Ω/\square) and ITO (15 Ω/\square)/PEN substrate in a chamber with 25% humidity at a spin speed of 2000 rpm for 30 s. The films were then annealed at 80 °C for 1 h at atmosphere of 25% humidity to remove residual organics and to obtain the a-quantized $\text{WO}_3\cdot\text{H}_2\text{O}$ films ($\text{WO}_3\cdot 80$). To confirm value of the WO_3 films can be prepared at a low temperature of 80 °C, other WO_3 -based films were prepared by annealing at 150 °C ($\text{WO}_3\cdot 150$) and 300 °C ($\text{WO}_3\cdot 300$) and their properties were compared with those of $\text{WO}_3\cdot 80$. In addition, to demonstrate the effectiveness of the novel approach of spontaneous hydrolysis in the fabrication of a-quantized $\text{WO}_3\cdot\text{H}_2\text{O}$ films, we fabricated films under 0% humidity conditions and compared their performances with that of the films prepared under 25% humidity conditions.

DSC (DSC-60, Shimadzu) was performed in the temperature range of 25–300 °C at a heating rate of 5 °C·min⁻¹ in air atmosphere. The chemical bonding states of the constituent elements were determined by XPS (AXIS ultra-delay line detector equipped with an Al K_{α} X-ray source, Korea Basic Science Institute, KBSI, Daedeok Headquarters) and FTIR spectroscopy (Nicolet iS50, Thermo Fisher Scientific). The surface morphologies were observed by FESEM (S – 4800, Hitachi). Raman spectroscopy was performed using a 532.1 nm laser excitation source. The film density was determined by the XRR. The electrical and optical properties were evaluated using a Hall-effect measurement system (Ecopia, HMS-3000) and by ultraviolet–visible (UV–vis) spectroscopy (Lambda – 35, Perkim – Elmer). The electronic structure was analyzed by UPS using an Axis ultra-delay line detector spectrometer (Kratos, UK) with a monochromatic Al K_{α} (1,486.6 eV) X-ray source and He I gas (21.22 eV) as a UV source.

The EC and electrochemical properties were measured in a three-electrode electrochemical cell containing 1 M LiClO_4 electrolyte with propylene carbonate as the solvent, Pt wire as the counter electrode, and Ag wire as the reference electrode using a potentiostat/galvanostat (PGSTAT302N, FRA32M, Metrohm Autolab B.V., the Netherlands), and by EIS. The EC energy-storage performance was determined *in situ* by a combination of potentiostat/galvanostat and UV–vis spectroscopy in a three-electrode electrochemical cell for a single flexible electrode and in a flexible solid-state cell assembled with LiClO_4 /PMMA-based electrolyte (2.5 M) and $\text{H}_2\text{PtCl}_6\cdot 6\text{H}_2\text{O}$ film (4 M, in terpineol) as the counter electrode. The bending tests of the flexible solid-state devices were performed using an all-electric dynamic test instrument (ElectroPulsTM E3000).

3. Results and discussion

Fig. 1a shows a novel formation mechanism of the a-quantized $\text{WO}_3\cdot\text{H}_2\text{O}$ films by the spontaneous hydrolysis of a spin-coated tungsten chloride (WOCl_6) solution reacted by H_2O molecules without a subsequent high-temperature annealing process. WOCl_6 reacts with 2-propanol ($\text{C}_3\text{H}_8\text{O}$) to form WOCl_4 molecules ($\text{WOCl}_6 + n\text{C}_3\text{H}_8\text{O} \rightarrow \text{W}(\text{OC}_3\text{H}_7)_n\text{Cl}_{6-n} + n\text{HCl}$, $\text{W}(\text{OR})\text{Cl}_5 \rightarrow \text{WOCl}_4 + \text{RCl}$) [25,26], which then undergo rapid hydrolysis and condensation with the H_2O molecules in the humid atmosphere of the chamber owing to its high reactivity with H_2O ,

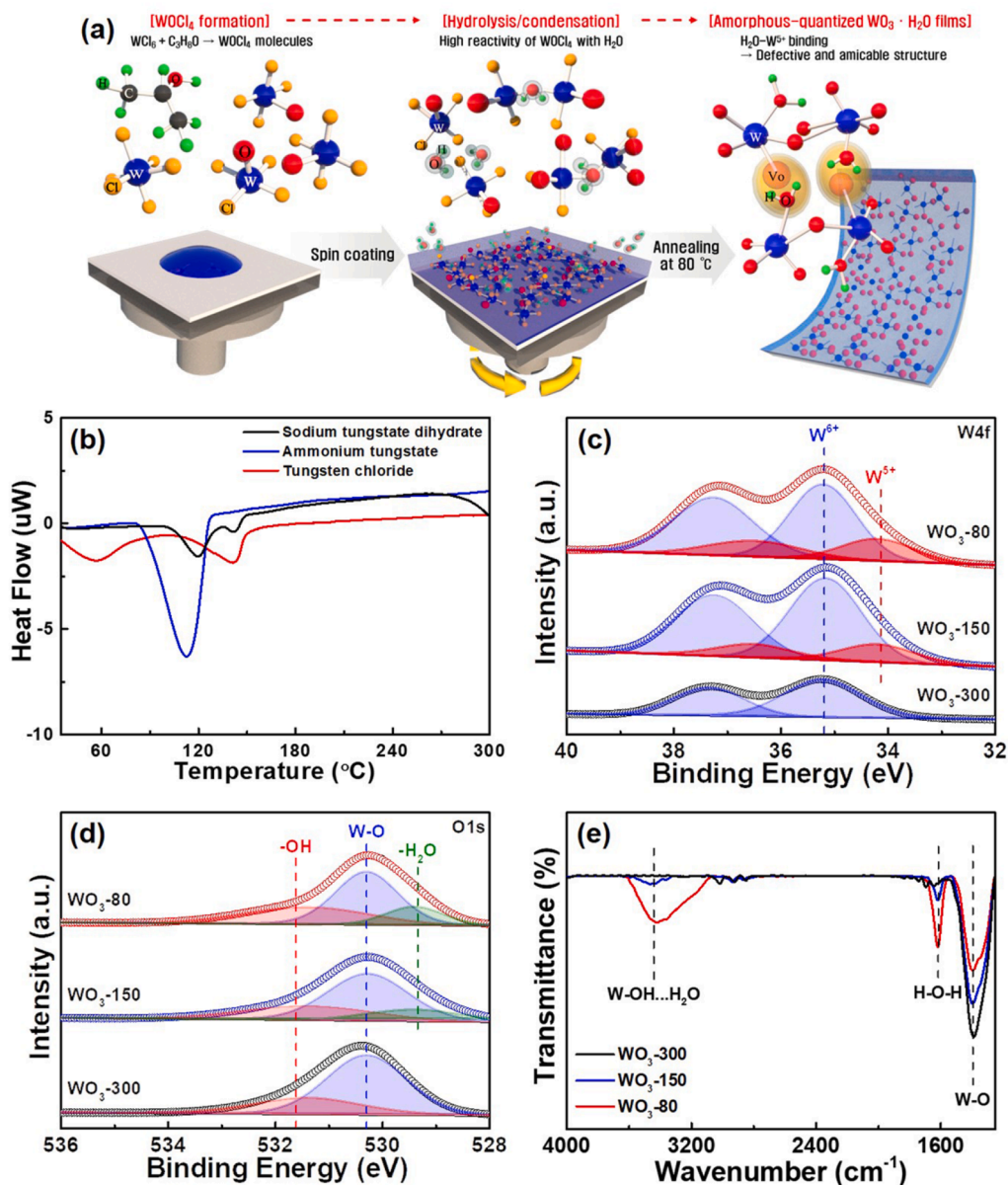


Fig. 1. (a) Schematic illustration of mechanism forming the a-quantized WO₃·H₂O films, (b) DSC curve of the precursor solutions measured in temperature range of 35–300 °C, and (c) W 4f and (d) O 1 s XPS spectras and (e) FTIR curve of all the films.

eventually forming WO₃·H₂O films on the substrates during the spin-coating process (Fig. S1a) [27,28]. This is a unique energy-efficient approach to fabricating flexible, high-performance electrodes on substrates without using excessive chemicals such as acids (e.g., HCl and citric acid) and/or high-temperature processes (>250 °C) [28–31]. The formation of a-quantized WO₃·H₂O films was evidenced by the appearance of an endothermic peak at 40–80 °C in the DSC curve corresponding to WCl₆ solution and the absence of peaks related to other precursors (Fig. 1b). The successful formation of a-quantized WO₃·H₂O films by this phenomenon was further verified by XPS and FTIR spectroscopic analyses of the films fabricated at different annealing temperatures. The W 4f XPS spectra (Fig. 1c) of WO₃-80, WO₃-150, and WO₃-300 exhibit two characteristic peaks at ~35.2 eV for W 4f_{7/2} and ~37.2 eV for W 4f_{5/2} corresponding to the binding energies of W⁶⁺ of the WO₃ phase [29,32]. The characteristic peaks at ~34.2 eV for W 4f_{7/2} and ~36.5 eV for W 4f_{5/2} correspond to W⁵⁺ related to oxygen vacancies (V_O) in the WO₃ phase. Interestingly, the W⁵⁺/W⁶⁺ peak ratio (0.23 for WO₃-150 and 0.32 for WO₃-80) increased with decreasing annealing temperature, which could be attributed to the H₂O molecules present in

the WO₃ lattice because of the low annealing temperature and can be a critical evidence of the generation of numerous V_O related to a-WO₃ quantization. The O 1 s XPS spectra of WO₃-300 (Fig. 1d) exhibited two characteristic peaks at ~530.2 and ~531.4 eV corresponding to W–O and –OH, while the O 1 s XPS spectra of WO₃-80 and WO₃-150 exhibited an additional peak at ~529.3 eV corresponding to –H₂O in addition to the two aforementioned characteristic peaks. The peak ratios of –OH/W–O (0.40, 0.46, and 0.59 for WO₃-300, WO₃-150, and WO₃-80, respectively) and –H₂O/W–O (0.28 and 0.31 for WO₃-150, WO₃-80, respectively) gradually increased with decreasing annealing temperature. This is in good agreement with the increase in the intensities of W–OH...H₂O peak at 3544.1 cm⁻¹ and H–O–H peak at 1,616.5 cm⁻¹, indicating the significant intercalation of H₂O molecules, as determined by FTIR spectroscopy (Fig. 1e). That is, a high annealing temperature of over 250 °C leads to the removal of H₂O molecules intercalated in the lattice and the incorporation of oxygen resulting in the formation of stoichiometric WO₃, as observed from the W 4f XPS results (Fig. 1c) and previous works on WO₃ [31,33]. However, in our study, as the H₂O molecules are the main reactant for WO₃ formation,

some of the molecules can absorb on transitional W^{5+} sites. Thus, the film before annealing at $80\text{ }^{\circ}\text{C}$ (Fig. S1c and d) is rich in W^{5+} and even W^{4+} owing to the presence of a large amount of absorbed H_2O molecules, which leads to the formation of $W-O$ bonds that impart blue color to the films (Fig. S1a). However, annealing at $80\text{ }^{\circ}\text{C}$ removes the physically absorbed molecules and supply oxygen to the unstable cationic sites, leading to the formation of H_2O-W^{5+} bonds with a bond length (2.37 \AA) similar to that of W^{6+} (2.38 \AA) in the typical WO_3 phase, and the films turn colorless (Fig. S1b) [34]. Therefore, an amicable structure with abundant defects can be beneficial for the electronic properties of the films and thus to put their electrochemical and optical performance toward a positive direction since the excess electrons are delocalized on the $5d$ orbitals of WO_3 [35].

Fig. 2a–c shows the top-view SEM images of the films prepared at different annealing temperatures. All the films have a homogenous structure with smooth and dense surfaces and no discernible particulates; this indicates the successful fabrication of the film with a thickness of $203.4\text{--}227.6\text{ nm}$ on the substrate (Fig. S2a and b) by the spontaneous hydrolysis of WCl_6 by the surrounding H_2O molecules. However, in the absence of H_2O molecules, the formation of the film structure (Fig. S2c and e) and the W^{6+} and H_2O related to the $WO_3\cdot H_2O$ phase is limited (Fig. S2d and e). Although the size of the grains constituting the films appear to decrease with decreasing annealing temperature, the effect of annealing temperature on the a- WO_3 phase was investigated in depth by Raman spectroscopy. The Raman spectra of all the films (Fig. 2d) exhibited a broad peak, which indicates the formation of a- WO_3 . This Raman peak was deconvoluted into three characteristic peaks corresponding to $W=O$ stretching mode (960 cm^{-1}) and $W-O$ stretching mode (807 and 719 cm^{-1}). According to Shigesato et al. and Hepel et al., the peak at 807 cm^{-1} indicates structural order with regard to the $W-O-W$ bond angle and length [36,37]. Therefore, the increase in $W=O/W-O$ peak ratio with increasing annealing temperature from $300\text{ }^{\circ}\text{C}$ to $80\text{ }^{\circ}\text{C}$ indicates the progressive amorphization of the film containing some defects, such as vacancies and interstitials, as a result of structural deformation due to the shortening and lengthening of the $W=O$ bond and the deficiency of $W-O$ bonds in a random network structure [34,38]. As other proof of the film amorphization, the XRD result (Fig. S3) shows that the full width at half maximum (FWHM) of broad peak related to amorphous nature is gradually widen from $WO_3\text{-}300$ to

$WO_3\text{-}80$, which corresponds to the decreased size of amorphous phases to induce the quantization [39,40]. This result can be affected to the film density directly related porosity. X-ray reflectometry (XRR) is important technique for measuring film density (ρ) from the critical angle (θ_c) measured from the reflected beam intensity, by Fresnel equation (Eq. (1)) [41]:

$$\theta_c = \sqrt{\frac{\gamma_0 \lambda^2}{\pi} N_A \frac{(z+f')}{A} \rho} \quad (1)$$

where γ_0 is the Bohr atomic radius, λ is the X-ray wavelength, N_A is Avogadro's number, Z is the number of electrons per atom, f' is the atomic scattering factor, and A is the atomic weight. As determined from the simulated XRR curve (Fig. 2e), the film density decreased with the decreasing annealing temperature ($\sim 5.6, 4.8,$ and 4.5 g cm^{-2} for $WO_3\text{-}300$, $WO_3\text{-}150$, and $WO_3\text{-}80$, respectively); this implies an increased in the number of electroactive sites on the films by amorphization. In typical a- WO_3 , the defects formed by the scarcity of $W=O$ and $W-O$ bonds can act as trapping sites for Li ions, which can negatively affect the electrochemical behavior [42]. However, because the scarcity of $W=O$ and $W-O$ bonds is compensated by the formation of $W-OH$ bonds by H_2O molecules (H_2O-W^{5+} bonds), a-quantized $WO_3\cdot H_2O$ has a stable structure despite its vacant cavities, which can facilitate efficient charge transfer and stress relief the during electrochemical reaction between electrons and Li ions at the electrode [43].

The new characteristics of a-quantized $WO_3\cdot H_2O$ are expected to improve its electrical and optical properties, which would be beneficial for its EC energy-storage performance. The first interesting property is the remarkable increase in the electrical conductivity of the film with decreasing annealing temperature (Fig. 3a and Table S1); the electrical conductivity of $WO_3\text{-}80$ was 2720 times of that of $WO_3\text{-}300$, which can be attributed to the increase in both carrier concentration and mobility. The increased carrier concentration is attributed to the addition of localized electrons in the d orbitals by the enrichment of W^{5+} with V_o , as determined from chemical formulae of $WO_3\text{-}150$ ($WO_{2.68}\cdot H_2O$) and $WO_3\text{-}80$ ($WO_{2.60}\cdot H_2O$). The localized electrons merged with the conduction band (CB) level and formed a continuum of states with a metallic character by shifting the Fermi level (E_F) close to the CB level, thereby improving the electrochemical activity of the films by acting as

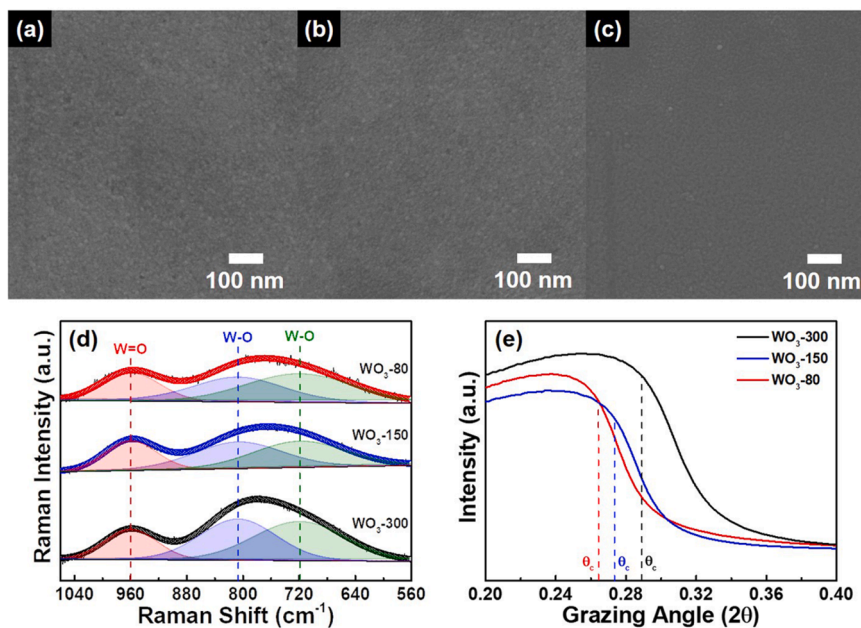


Fig. 2. Top-view SEM images of the films prepared with different annealing temperature ((a) $WO_3\text{-}300$, (b) $WO_3\text{-}150$, and (c) $WO_3\text{-}80$) and (d) Raman and (e) XRR curves of all the films.

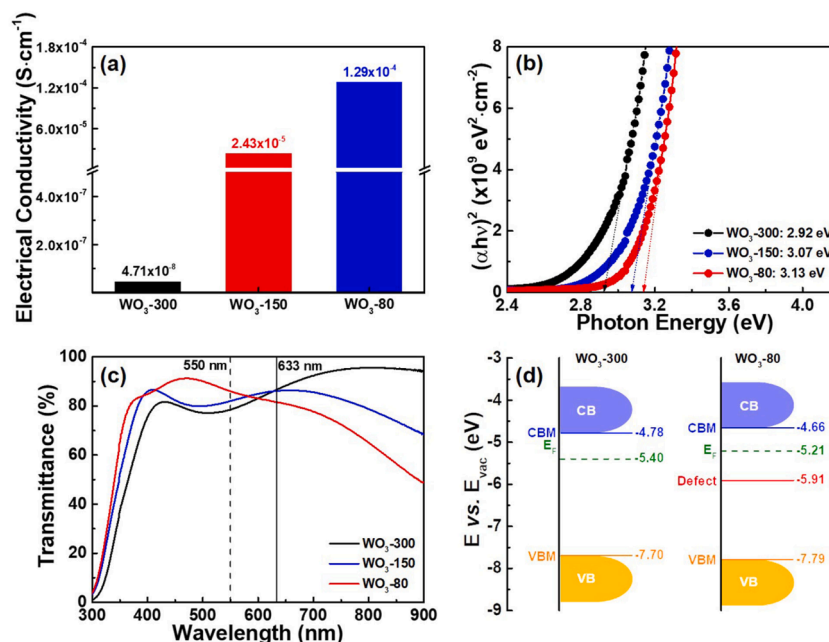


Fig. 3. (a) Electrical conductivity, (b) plot of $(\alpha h\nu)^2$ versus photon energy, (c) optical transmittance curve of all the films, and (d) schematic illustration of energy band structure for comparison between WO_3 -300 and WO_3 -80.

reactive sites [25,44]. In addition, the high Hall mobility can be attributed to the amicable electronic structure of a-quantized $\text{WO}_3\cdot\text{H}_2\text{O}$, as confirmed from Urbach energy (E_U), which is related to the degree of disorder of the films by Eq. (2) [45,46]:

$$\alpha = \alpha_0 \exp(h\nu/E_U) \quad (2)$$

where α is the absorption coefficient and $h\nu$ is the photon energy. The E_U found below the absorption band edge of the compound is governed by the deformation of phonon states in the film resulting from structural disorder [46]. The gradual decrease in E_U (Fig. S4a) indicates the relaxation of film distortion in the case of WO_3 -80 due to the compensatory interaction of the longer W-OH bond, which can be the main reason for high Hall mobility in the films. The transmittance curves (Fig. 3c) exhibited distinct differences in the transmittance of the films fabricated at different annealing temperatures; the result indicates the suitability of the film for EC energy-storage devices. The optical transmittance of the films decreases with increasing annealing temperature narrowing of optical band gap (E_g) due to some structural effects such as improved grain size or lattice deficiency in the films [47,48]. However, since abundant V_o can widen the E_g (Fig. 3b), the transmittance peak at

300–600 nm blue-shifted, while the intensity of the peak at 600–900 nm decreased due to significant carrier scattering (Fig. 3c). To determine the reason for the unique transmittance behavior, we compared the energy band structures of the WO_3 -300 and WO_3 -80, by integrating the E_F values determined by ultraviolet photoelectron spectroscopy (UPS) with a photon energy of 21.22 eV (Fig. S4b), E_g (Fig. 3b), and valence band maximum (VBM, Fig. S4c and d). Unlike WO_3 -300, the energy band structure of WO_3 -80 indicates the widening of E_g due to the shifting of CBM to a higher energy because of the high electron density of the CB. Consequently, the E_F shifted toward the CBM and a new defect level formed at -5.91 eV in the E_g , which is consistent with the quantization of crystalline WO_3 with abundant V_o (Fig. 3d) [44,49]. The results indicate an original concept for the quantization of a- WO_3 owing to the formation of abundant V_o in the electronic structure, which is beneficial for improving device to transparency as well as electrochemical reaction capacity and kinetics.

Fig. 4a shows the cyclic voltammetry (CV) curves of the electrodes prepared with the WO_3 films fabricated at different annealing temperatures measured in the voltage range of -0.7 to 1.0 V at a scan rate of 20 $\text{mV}\cdot\text{s}^{-1}$. All the electrodes exhibited a broad redox curve without any

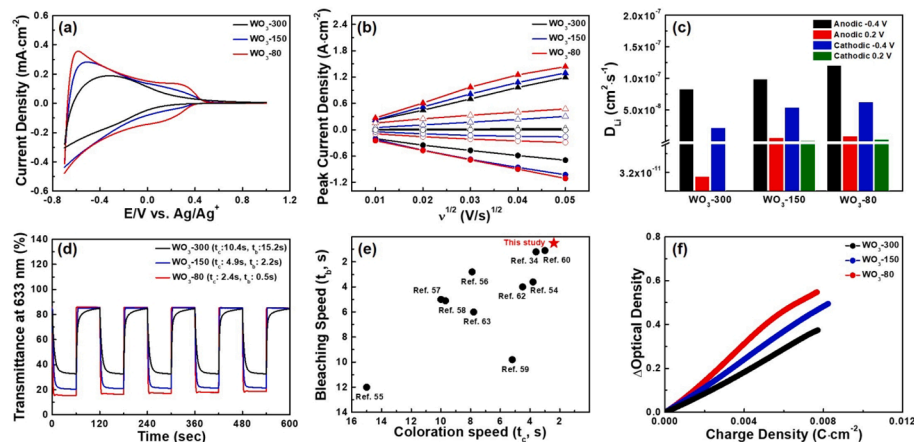


Fig. 4. (a) CV curve of all electrodes prepared with different annealing temperature measured in the three-electrode system by applying potential range from -0.7 to 1.0 V at a 20 mV/s scan rate, (b) plots of peak current density (J_p) with respect to the varied scan rates for all electrodes under cathodic reactions (filled circle for -0.4 V and empty circle for 0.2 V) and anodic reactions (filled triangle for -0.4 V and empty triangle for 0.2 V), (c) calculated Li-ion diffusion coefficient (D_{Li}) at different potential, (d) *in situ* transmittance curve of all electrodes between coloured state and bleached state at stepping potential of -0.7 V and 1.0 V for 60 s with a wavelength of 633 nm, (e) comparative plot of the switching performances on WO_3 -80 with previous WO_3 -based reports, and (f) plot showing OD versus applied charge density when all electrodes are under steady potential of -0.7 V.

sharp peaks corresponding to the EC behavior of a-WO₃, and the area of hysteresis loop gradually increased with increasing current density over the applied potential range in the order of WO₃-300 < WO₃-150 < WO₃-80 electrode, indicating an increase in electrochemical activity resulting in the insertion/extraction of more Li ions from the active material due to the presence of abundant V_o acting as reactive sites for Li ions [50]. The redox current densities of the electrodes above 0 V increased with decreasing annealing temperature, which can be attributed to the H₂O molecules in a-WO₃ providing fresh electrochemical sites, thereby improving the EC energy-storage performance. This was confirmed from the unique chemical binding state of the inserted Li ions on the a-quantized WO₃-H₂O films under sequentially applied cathodic potentials of 0.2 V and -0.4 V. While the cathodic reaction of typical WO₃ involves the chemical binding of Li₂O resulting in coloring or charging of the electrode, the cathodic curves of a-quantized WO₃-H₂O films (0.2 V, Fig. S5) exhibited a dominant peak corresponding to interstitial Li (Li_i, 84.6%) along with a minor peak related to Li₂O (15.4%). In addition, the Li₂O peak (Li-O, 21.3%) became more intense at cathodic -0.4 V, indicating the typical Li-insertion process of a-WO₃. Therefore, unlike basic WO₃, the presence of Li_i in the a-quantized WO₃-H₂O films can be a crucial evidence of the presence of a large number of electroactive sites for Li insertion due to structural interaction between the V_o and H₂O molecules in a-WO₃ [43,50]. In addition, the Li-ion diffusion coefficient (D_{Li}) of the WO₃-80 electrode, calculated from the plot of peak current density (J_p) and versus the square root of scan rate (C₀), was significantly high at cathodic (-0.4 V) and anodic (-0.4 V) reactions, together with even one at 0.2 V related to the H₂O molecule (Fig. 4b and 4c with Table S2), indicating fast electrochemical kinetics at Li-O and Li_i due to

the synergistic effect of increased number of electroactive sites and enhanced electrical conductivity [37,51]. Therefore, as shown in Fig. 4d, the strong electrochemical activity widened the transmittance modulation ($\Delta T = 70.5\%$ at 633.0 nm) and increased the switching speeds (2.4 s for coloration: t_c and 0.5 s for bleaching: t_b) of the WO₃-80 electrode. Consequently, the WO₃-80 electrode exhibited the best switching performance compared with that of the other films and previously reported WO₃-based electrodes (Table S3 and Fig. 4e) [29,52-59]. Moreover, compared with the other films, the WO₃-80 electrode exhibited the highest coloration efficiency (CE), which is an important parameter for the comprehensive assessment of EC devices (Fig. 4f) and can be calculated from optical density (OD) and applied charge density (Q/A) by Eqs. (3) and (4) [60]:

$$CE = \Delta OD / (Q/A) \quad (3)$$

$$\Delta OD = \log(T_b/T_c) \quad (4)$$

The performance improvement is mainly ascribed to the synergistic effect of the wide transmittance modulation due to the improved electrochemical activity and efficient charge transport because of the increases in electrical conductivity and D_{Li}.

The EC energy-storage performance was evaluated using single flexible electrodes formed by spin coating the a-quantized WO₃-H₂O films on an indium tin oxide (ITO)/PEN substrate under 25% humidity conditions (hereafter referred as WO₃-80/25%). To determine the effect of humidity on the formation of a-quantized WO₃-H₂O films, the performance of WO₃-80 films prepared under 0% humidity conditions (WO₃-80/0%) was also evaluated. CV was performed in the potential

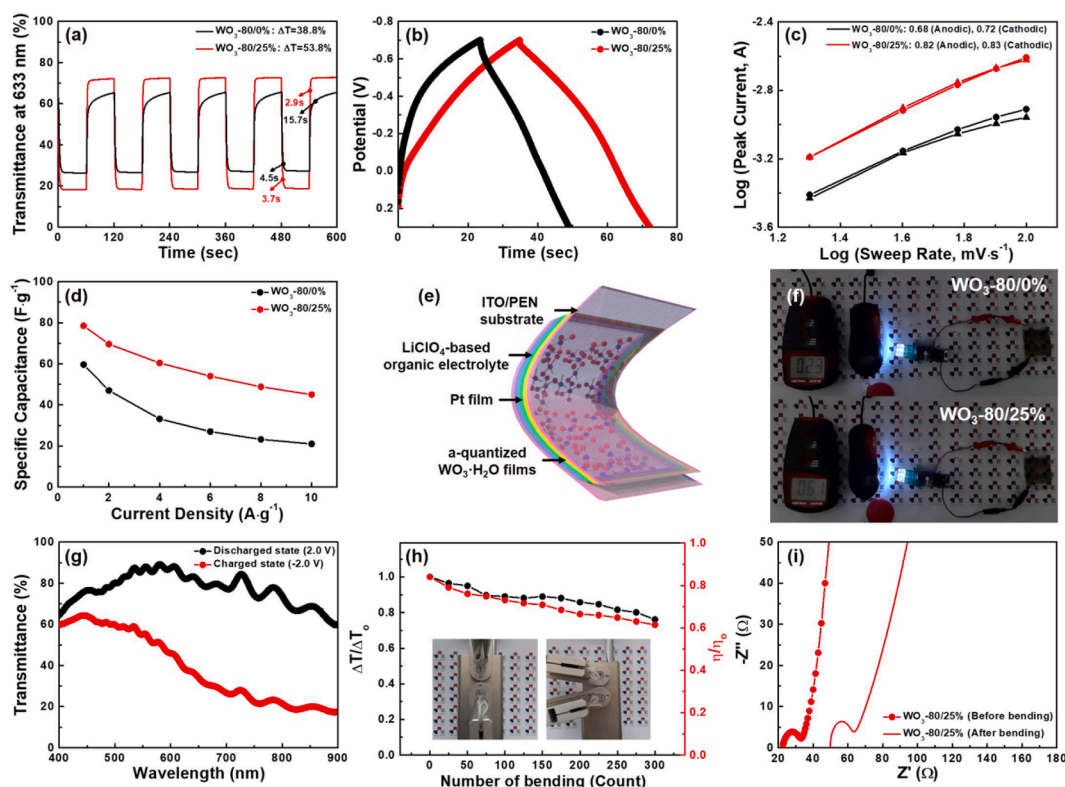


Fig. 5. (a) Comparison of *in situ* transmittance curve between WO₃-80/25% and WO₃-80/0% flexible electrodes, (b) galvanostatic charge/discharge curves of the flexible electrodes traced at current density of 1 A/g in potential range from -0.7 to 0.3 V, (c) determination of the *b*-values (filled circle for cathodic -0.4 V and filled triangle for anodic -0.4 V) using the relation ($i = av^b$) between current (*i*) and sweep rate (*v*) in the CV curves, (d) plot of specific capacitance as a function of the current density, (e) schematic illustration of the structure of the flexible solid-state devices with both EC and energy-storage, (f) real photograph of the flexible solid-state devices that are lighting 1.5 V white LED, (g) transmittance curve in wavelength range of 400–900 nm as the result of discharged and charged states (h) variation of transmittance at 633 nm and specific capacitance at 1 A/g current density versus repetitive bending cycles with a curvature radius of 1.3 cm (inserted photographs of mechanical bending processes on the flexible solid-state devices), and (i) comparison of the EIS curves between before and after bending processes of 300 cycles.

range of -0.7 to 0.3 V at a scan rate of 20 mV s $^{-1}$, and the results are shown in Fig. S6a. As can be seen, the electrochemical activity of the WO $_3$ -80/25% flexible electrode is considerably higher than that of the WO $_3$ -80/0% electrodes, as determined from the wide CV curve area of the WO $_3$ -80/25% electrode, indicating the increase in ΔT (Fig. 5a). In addition, the WO $_3$ -80/25% flexible electrode exhibited competitive switching speeds. While both electrodes exhibited high switching speeds for the coloration process because of the presence of abundance V_o , the bleaching speed of the WO $_3$ -80/25% flexible electrode was higher than that of the WO $_3$ -80/0% electrode, which can be attributed to H $_2$ O molecules that stabilized the a-WO $_3$ structure with abundant V_o despite the low annealing temperature. In contrast, in the absence of H $_2$ O molecules, the V_o were a major drawback in the trapping of Li ions. Hence, the D_{Li} (0.81×10^{-8} cm 2 s $^{-1}$) of the WO $_3$ -80/0% flexible electrode during the anodic process was the lowest (1.03×10^{-8} cm 2 s $^{-1}$ for the cathodic process of the WO $_3$ -80/0% flexible electrode, and 2.57×10^{-8} and 2.80×10^{-8} cm 2 s $^{-1}$ for the anodic and cathodic processes of the WO $_3$ -80/25% flexible electrode, respectively), as shown in Fig. S6b. The energy-storage performance of the flexible electrodes used as a supercapacitor was evaluated by galvanostatic charge–discharge (GCD) measurements performed at a current density of 1 A g $^{-1}$ (Fig. 5b). The symmetric triangular shape of GCD curves indicates a pseudocapacitive behavior and good electrochemical reversibility of the electrodes [51,61]. The GCD curves of the WO $_3$ -80/25% flexible electrode are more symmetrical than those of the WO $_3$ -80/0% flexible electrode, which indicates the higher energy-storing capacity and good electrochemical reversibility of the WO $_3$ -80/25% flexible electrode owing to its remarkably high electrochemical activity and kinetics. This was further used to determine the type of contribution (capacitive ($b \approx 1$) or diffusive ($b \approx 0.5$)) from the relation $i = av^b$ where i is the current and v is the sweep rate in the CV curves. As shown in Fig. 5c, the calculated b values of the a-quantized WO $_3$ -H $_2$ O films (WO $_3$ -80/25% flexible electrode) are close to 1, which suggest that their fast is because of the dominant surface capacitive insertion/extraction processes [62,63]. Hence, the improved electrochemical activity of the WO $_3$ -80/25% flexible electrode owing to the increased number of electroactive sites of the a-quantized WO $_3$ -H $_2$ O films resulted in a higher specific capacitance (78.5 F g $^{-1}$) compared with that of the WO $_3$ -80/0% flexible electrode (59.6 F g $^{-1}$). In addition, the WO $_3$ -80/25% flexible electrode exhibited a high rate capability with 57.3% specific capacitance retention with an increase in current density from 1 to 10 A g $^{-1}$, while WO $_3$ -80/0% exhibited a low capacitance retention of 35.2%, which is mainly ascribed to the increase in electrical conductivity and D_{Li} of the a-quantized WO $_3$ -H $_2$ O films (Fig. 5d). To confirm the practical applicability of the flexible multifunctional devices with both EC and energy-storage functions, a a-quantized WO $_3$ -H $_2$ O film (WO $_3$ -80/25%) coated on an ITO/PEN substrate as an active material was assembled into a solid-state cell composed of a Pt-coated ITO/PEN substrate as the counter electrode and a gel polymer electrolyte (PMMA + LiClO $_4$ + PC), as illustrated in Fig. 5e. The charged colored device could light a 1.5 V white light-emitting diode (LED, FK185, 1.5 V 6-LED LIGHT) (Fig. 5f), and upon discharge, the device became colorless (bleaching condition), and the LED dimmed. Thus, the flexible device allows the visual monitoring of the amount of energy stored in it through color variation. This was further confirmed by the successive variation of transmittance under an applied potential; the dark-blue devices exhibited 37.3% transmittance at 633 nm in a fully charged state of -2.0 V and turned colorless with 82.5% transmittance at 633 nm upon discharge to 2.0 V (Fig. 5g). In particular, the illumination intensity of the LEDs powered by the WO $_3$ -80/25% flexible electrode was higher than that of the LED powered by the WO $_3$ -80/0% flexible electrode, which can be attributed to the higher energy density improved owing to the higher electrochemical activity of WO $_3$ -80/25% (Fig. S6c). The applicability of flexible EC energy-storage devices comprising the a-quantized WO $_3$ -H $_2$ O films was evaluated ex-situ by examining the device performance over 300 bending cycles. As shown in Fig. 5h, the devices bent to a bending

radius of 1.3 cm maintained their good performance with 76.1% ΔT and 73.1% specific capacitance after 300 cycles as the realization of the normal charging and discharging processes (see Fig. S7), which can be attributed to the competitive tolerance of the a-quantized WO $_3$ -H $_2$ O films in maintaining the charge-transfer resistance of the electrodes, as confirmed by EIS (Fig. 5i) despite the increase in series resistance due to the damage of the ITO/PEN substrate used as a transparent conducting electrode because of the presence of defective sites for mechanical stress relaxation. In addition, this behavior brings about the competitive cycling stabilities (transmittance retention of 85.90% after 1000-consecutive coloration-bleaching and capacitance retention of 86.5% after 1000 charging and discharging reactions at current density of 1 A/g) as the flexible electrode for the EC energy-storage devices (see Fig. S8). Considering that our study is the first to propose a low-temperature synthetic process for a-WO $_3$ films that can be directly used in flexible multifunctional devices as an active material, the results are indeed encouraging and desirable.

Based on the unique results, we propose a possible mechanism for the a-quantized WO $_3$ -H $_2$ O films for the realization and performance improvement of flexible EC energy-storage devices. The a-quantized WO $_3$ -H $_2$ O films have an amicable structure with abundant defective states because of the unique interaction between the intercalated H $_2$ O molecules and transitional W $^{5+}$ in a-WO $_3$, despite a low annealing temperature of 80 °C. As an attractive characteristic, the fabricated film has a defective structure, which is conducive to increasing the number of the electroactive sites by the deformation of the bonds between W and O due to amorphization. However, the presence of H $_2$ O molecules stabilizes the structure, leading to efficient charge transfer and stress alleviation during electrochemical reactions; consequently, the ΔT and specific capacitance of the flexible multifunctional devices are improved and could be visually monitored. In addition, since the abundant V_o result in the quantization of the a-WO $_3$ electronic structure, the electrical conductivity related to the electrochemical kinetics of the film increased owing to the increases in both carrier concentration and mobility, which resulted rapid switchability and high rate capability of the flexible EC energy-storage devices. Therefore, we strongly believe that our study provides new comprehensive foundation for the development of active electrodes for flexible EC energy-storage devices.

4. Conclusions

In summary, we developed an advanced flexible electrode based on a-quantized WO $_3$ -H $_2$ O films fabricated by the spontaneous hydrolysis of spin-coated WCl $_6$ solution by H $_2$ O molecules in the surrounding atmosphere at a low-annealing temperature of 80 °C. The new low-temperature process provides an efficient framework with improved performance and a wide application scope, which cannot be achieved with high-temperature synthetic processes. During the synthesis of a-quantized WO $_3$ -H $_2$ O films, the H $_2$ O molecules triggered the hydrolysis and condensation of WOCl $_4$ molecules to form the a-WO $_3$ phase and provided abundant defective states and stabilized the deficient chemical structure of the films, resulting in the quantization of a-WO $_3$ having numerous electroactive sites, abundant V_o , and a wide E_g . The a-quantized WO $_3$ -H $_2$ O films exhibited efficient charge transfer and stress alleviation during electrochemical reactions, which resulted in the activation of ΔT modulation (70.5% on a rigid fluorine-doped tin oxide (FTO) substrate and 53.8% on a flexible ITO/PEN substrate) and specific capacitance (78.5 F g $^{-1}$ at current density of a 1 A/g $^{-1}$ on a flexible ITO/PEN substrate) for EC energy-storage devices. Moreover, the devices maintained their good performance (76.1% ΔT and 73.1% specific capacitance) even after 300 bending cycles at a bending radius of 1.3 cm. Furthermore, the increase in electrical conductivity of the electrode due to increase in carrier concentration and mobility, resulted in the rapid switchability (2.4 s for coloration and 0.5 s for bleaching on a rigid FTO substrate and 3.7 s for coloration and 2.9 s for bleaching on flexible ITO/PEN substrate) and higher rate capability of the multifunctional

devices. Such low-temperature-synthesized a-quantized $\text{WO}_3\text{-H}_2\text{O}$ films can offer new possibilities for the design and development of active electrodes for flexible EC energy-storage devices.

Declaration of Competing Interest

The authors declare that they have no known competing financial interests or personal relationships that could have appeared to influence the work reported in this paper.

Acknowledgements

This work was supported by the National Research Foundation of Korea (NRF) grant funded by the Korea government (MSIT) (No. 2019R1A2C1005836).

Appendix A. Supplementary data

Supplementary data to this article can be found online at <https://doi.org/10.1016/j.cej.2021.130383>.

References

- [1] S. Xie, Y. Chen, Z. Bi, S. Jia, X. Guo, X. Gao, X. Li, Energy storage smart window with transparent-to-dark electrochromic behavior and improved pseudocapacitive performance, *Chem. Eng. J.* 370 (2019) 1459–1466, <https://doi.org/10.1016/j.cej.2019.03.242>.
- [2] J.P. Cheng, W.D. Wang, X.C. Wang, F. Liu, Recent research of core-shell structured composites with NiCo_2O_4 as scaffolds for electrochemical capacitors, *Chem. Eng. J.* 393 (2020) 124747, <https://doi.org/10.1016/j.cej.2020.124747>.
- [3] B.-R. Koo, K.-W. Sung, H.-J. Ahn, Boosting ultrafast lithium storage capability of hierarchical core/shell constructed carbon nanofiber/3D interconnected hybrid network with nanocarbon and FTO nanoparticles heterostructures, *Adv. Funct. Mater.* 30 (2020) 2001863, <https://doi.org/10.1002/adfm.202001863>.
- [4] B.-R. Koo, D.-H. Oh, D.-H. Riu, H.-J. Ahn, Improvement of transparent conducting performance on oxygen-activated fluorine-doped tin oxide electrodes formed by horizontal ultrasonic spray pyrolysis deposition, *ACS Appl. Mater. Interfaces* 9 (51) (2017) 44584–44592, <https://doi.org/10.1021/acsami.7b12968>.
- [5] Q. Guo, X. Zhao, Z. Li, D. Wang, G. Nie, A novel solid-state electrochromic supercapacitor with high energy storage capacity and cycle stability based on poly(5-formylindole)/ WO_3 honeycombed porous nanocomposites, *Chem. Eng. J.* 384 (2020) 123370, <https://doi.org/10.1016/j.cej.2019.123370>.
- [6] Y.-H. Lee, J.S. Kang, J.-H. Park, J. Kang, I.-R. Jo, Y.-E. Sung, K.-S. Ahn, Color-switchable electrochromic $\text{Co}(\text{OH})_2/\text{Ni}(\text{OH})_2$ nanofilms with ultrafast kinetics for multifunctional smart windows, *Nano Energy* 72 (2020) 104720, <https://doi.org/10.1016/j.nanoen.2020.104720>.
- [7] H.-e. Zhang, Y. Tian, S. Wang, Y. Huang, J. Wen, C. Hang, Z. Zheng, C. Wang, Highly stable flexible transparent electrode via rapid electrodeposition coating of Ag-Au alloy on copper nanowires for bifunctional electrochromic and supercapacitor device, *Chem. Eng. J.* 399 (2020) 125075, <https://doi.org/10.1016/j.cej.2020.125075>.
- [8] E.D. Martínez, C.D.S. Brites, L.D. Carlos, A.F. García-Flores, R.R. Urbano, C. Rettori, Electrochromic switch devices mixing small- and large-sized upconverting nanocrystals, *Adv. Funct. Mater.* 29 (8) (2019) 1807758, <https://doi.org/10.1002/adfm.2019.29.8.1807758>.
- [9] L. Shen, L. Du, S. Tan, Z. Zang, C. Zhao, W. Mai, Flexible electrochromic supercapacitor hybrid electrodes based on tungsten oxide films and silver nanowires, *Chem. Commun.* 52 (37) (2016) 6296–6299, <https://doi.org/10.1039/C6CC01139J>.
- [10] H. Wang, C.-J. Yao, H.-J. Nie, L. Li, Yang, S. Mei, Q. Zhang, Recent progress in integrated functional electrochromic energy storage devices, *J. Mater. Chem. C* 8 (44) (2020) 15507–15525, <https://doi.org/10.1039/D0TC03934A>.
- [11] G. Cai, J. Chen, J. Xiong, A. Lee-Sie Eh, J. Wang, M. Higuchi, P.S. Lee, Molecular level assembly for high-performance flexible electrochromic energy-storage devices, *ACS Energy Lett.* 5 (4) (2020) 1159–1166, <https://doi.org/10.1021/acscenergylett.0c00245>.
- [12] C. Wang, Z. Wang, Y. Ren, X. Hou, F. Yan, Flexible electrochromic Zn mirrors based on Zn/Viologen hybrid batteries, *ACS Sustainable Chem. Eng.* 8 (13) (2020) 5050–5055, <https://doi.org/10.1021/acssuschemeng.9b06818>.
- [13] K. Zhou, H. Wang, J. Jiu, J. Liu, H. Yan, K. Sugauma, Polyaniline films with modified nanostructure for bifunctional multicolor electrochromic and supercapacitor applications, *Chem. Eng. J.* 345 (2018) 290–299, <https://doi.org/10.1016/j.cej.2018.03.175>.
- [14] S. Huang, Y. Liu, M. Jafari, M. Sijah, H. Wang, S. Xiao, D. Ma, Highly stable Ag-Au core-shell nanowire network for ITO-free flexible organic electrochromic device, *Adv. Funct. Mater.* 31 (14) (2021) 2010022, <https://doi.org/10.1002/adfm.202010022>.
- [15] M.A. Shinde, H. Kim, Highly stable silver nanowire-based transparent conductive electrodes for electrochromic devices, *Mater. Today Commun.* 26 (2021) 102147, <https://doi.org/10.1016/j.mtcomm.2021.102147>.
- [16] S. Kiruthika, G.U. Kulkarni, Smart electrochromic supercapacitors made of metal mesh electrodes with polyaniline as charge storage indicator, *Energy Technol.* 8 (5) (2020) 1901364, <https://doi.org/10.1002/ente.v8.5.1002/ente.201901364>.
- [17] Z. Bi, X. Li, Y. Chen, X. Xu, S. Zhang, Q. Zhu, Bi-functional flexible electrodes based on tungsten trioxide/zinc oxide nanocomposites for electrochromic and energy storage applications, *Electrochim. Acta* 227 (2017) 61–68, <https://doi.org/10.1016/j.electacta.2017.01.003>.
- [18] B.G. Rao, D. Mukherjee, B.M. Reddy, Chapter 1 - Novel approaches for preparation of nanoparticles, *Nanostructures for Novel Therapy 1* (2017) 1–36. <https://doi.org/10.1016/B978-0-323-46142-9.00001-3>.
- [19] L. Zhang, D. Chao, P. Yang, L. Weber, J. Li, T. Kraus, H.J. Fan, Flexible pseudocapacitive electrochromics via inkjet printing of additive-free tungsten oxide nanocrystal ink, *Adv. Energy Mater.* 10 (17) (2020) 2000142, <https://doi.org/10.1002/aenm.v10.17.1002/aenm.202000142>.
- [20] C. Costa, C. Pinheiro, I. Henriques, C.A.T. Laia, Inkjet printing of sol-gel synthesized hydrated tungsten oxide nanoparticles for flexible electrochromic devices, *ACS Appl. Mater. Interfaces* 4 (3) (2012) 1330–1340, <https://doi.org/10.1021/am201606m>.
- [21] Z. Bi, X. Li, Y. Chen, X. He, X. Xu, X. Gao, Large-scale multifunctional electrochromic-energy storage device based on tungsten trioxide monohydrate nanosheets and Prussian white, *ACS Appl. Mater. Interfaces* 9 (35) (2017) 29872–29880, <https://doi.org/10.1021/acsami.7b08656>.
- [22] Y. Ke, J. Chen, G. Lin, S. Wang, Y. Zhou, J. Yin, P.S. Lee, Y.i. Long, Smart windows: electro-, thermo-, mechano-, photochromics, and beyond, *Adv. Energy Mater.* 9 (39) (2019) 1902066, <https://doi.org/10.1002/aenm.v9.39.1002/aenm.201902066>.
- [23] S.P. Gupta, H.H. Nishad, V.B. Patil, S.D. Chakane, M.A. More, D.J. Late, P.S. Walke, Morphology and crystal structure dependent pseudocapacitor performance of hydrated WO_3 nanostructures, *Mater. Adv.* 1 (7) (2020) 2492–2500, <https://doi.org/10.1039/D0MA00518E>.
- [24] N. Zhang, X. Li, Y. Liu, R. Long, M. Li, S. Chen, Z. Qi, C. Wang, L.i. Song, J. Jiang, Y. Xiong, Defective tungsten oxide hydrate nanosheets for boosting aerobic coupling of amines: synergistic catalysis by oxygen vacancies and Brønsted acid sites, *Small* 13 (31) (2017) 1701354, <https://doi.org/10.1002/sml.v13.31.1002/sml.201701354>.
- [25] V.A. Khodzhemirov, V.A. Yevdokimova, V.M. Cherednichenko, Reaction of WCl_6 with alcohols and the activity of the resulting catalysts in polymerization of cyclopentene, *Polym. Sci. U.S.S.R.* 18 (3) (1976) 581–588, [https://doi.org/10.1016/0032-3950\(76\)90250-1](https://doi.org/10.1016/0032-3950(76)90250-1).
- [26] W.C. Fernelius, *Inorganic syntheses*, McGraw-Hill, New York 3 (1950).
- [27] K. Bergum, A. Magras, H. Fjellvåg, O. Nilsen, Thin film fabrication and characterization of proton conducting lanthanum tungstate, *J. Mater. Chem. A* 2 (43) (2014) 18463–18471, <https://doi.org/10.1039/C4TA03359K>.
- [28] P. Judeinstein, J. Livage, Sol-gel synthesis of WO_3 thin films, *J. Mater. Chem.* 1 (4) (1991) 621–627, <https://doi.org/10.1039/JM9910100621>.
- [29] Y. Yao, Q.i. Zhao, W. Wei, Z. Chen, Y. Zhu, P. Zhang, Z. Zhang, Y. Gao, WO_3 quantum-dots electrochromism, *Nano Energy* 68 (2020) 104350, <https://doi.org/10.1016/j.nanoen.2019.104350>.
- [30] K. Wenderich, J. Noack, A. Kärger, A. Trunschke, G. Mul, Effect of temperature and pH on phase transformations in citric acid mediated hydrothermal growth of tungsten oxide, *Eur. J. Inorg. Chem.* 2018 (7) (2018) 917–923, <https://doi.org/10.1002/ejic.201701156>.
- [31] J.J. Qi, S. Gao, K. Chen, J. Yang, H.W. Zhao, L. Guo, S.H. Yang, Vertically aligned, double-sided, and self-supported 3D WO_3 nanocolumn bundles for low-temperature gas sensing, *J. Mater. Chem. A* 3 (35) (2015) 18019–18026, <https://doi.org/10.1039/C5TA03711E>.
- [32] K.-H. Kim, B.-R. Koo, H.-J. Ahn, Effects of Sb-doped $\text{SnO}_2\text{-WO}_3$ nanocomposite on electrochromic performance, *Ceram. Int.* 45 (13) (2019) 15990–15995, <https://doi.org/10.1016/j.ceramint.2019.05.109>.
- [33] A.K. Nayak, Y. Sohn, D. Pradhan, Facile green synthesis of $\text{WO}_3\text{-H}_2\text{O}$ nanoplates and WO_3 nanowires with enhanced photoelectrochemical performance, *Cryst. Growth Des.* 17 (9) (2017) 4949–4957, <https://doi.org/10.1021/acs.cgd.7b00886>.
- [34] E. Albanese, C. Di Valentini, G. Pacchioni, H_2O adsorption on WO_3 and WO_{3-x} (001) surfaces, *ACS Appl. Mater. Interfaces* 9 (27) (2017) 23212–23221, <https://doi.org/10.1021/acsami.7b06139>.
- [35] Y. Shigesato, A. Murayama, T. Kamimori, K. Matsuhiro, Characterization of evaporated amorphous WO_3 films by Raman and FTIR spectroscopies, *Appl. Surf. Sci.* 33 (1988) 804–811, [https://doi.org/10.1016/0169-4332\(88\)90384-4](https://doi.org/10.1016/0169-4332(88)90384-4).
- [36] M. Hepel, H. Redmond, Large cation model of dissociative reduction of electrochromic WO_{3-x} films, *Cent. Eur. J. Chem.* 7 (2009) 234–245, <https://doi.org/10.2478/s11532-009-0009-z>.
- [37] Y.S. Krasnov, G.Y. Kolbasov, Electrochromism and reversible changes in the position of fundamental absorption edge in cathodically deposited amorphous WO_3 , *Electrochim. Acta* 49 (15) (2004) 2425–2433, <https://doi.org/10.1016/j.electacta.2004.01.020>.
- [38] A. Antonaia, M.C. Santoro, G. Farnelli, T. Polichetti., Transport mechanism and IR structural characterisation of evaporated amorphous WO_3 films, *Thin Solid Films* 426 (1-2) (2003) 281–287, [https://doi.org/10.1016/S0040-6090\(03\)00011-7](https://doi.org/10.1016/S0040-6090(03)00011-7).

- [39] K.P. Regan, C. Koenigsmann, S.W. Sheehan, S.J. Konezny, C.A. Schmuttenmaer, Size-dependent ultrafast charge carrier dynamics of WO₃ for photoelectrochemical cells, *J. Phys. Chem. C* 120 (27) (2016) 14926–14933, <https://doi.org/10.1021/acs.jpcc.6b04390>.
- [40] A. Wolcott, T.R. Kuykendall, W. Chen, S. Chen, J.Z. Zhang, Synthesis and characterization of ultrathin WO₃ nanodisks utilizing long-chain poly(ethylene glycol), *J. Phys. Chem. B* 110 (50) (2006) 25288–25296, <https://doi.org/10.1021/jp064777b10.1021/jp064777b.s001>.
- [41] E. Chason, T.M. Mayer, Thin film and surface characterization by specular X-ray reflectivity, *Crit. Rev. Solid State Mat. Sci.* 22 (1) (1997) 1–67, <https://doi.org/10.1080/10408439708241258>.
- [42] W. Cheng, J. He, K.E. Dettelbach, N.J.J. Johnson, R.S. Sherbo, C.P. Berlinguette, Photodeposited amorphous oxide films for electrochromic windows, *Chem* 4 (4) (2018) 821–832, <https://doi.org/10.1016/j.chempr.2017.12.030>.
- [43] G. Cai, M. Cui, V. Kumar, P. Darmawan, J. Wang, X.u. Wang, A. Lee-Sie Eh, K. Qian, P.S. Lee, Ultra-large optical modulation of electrochromic porous WO₃ film and the local monitoring of redox activity, *Chem. Sci.* 7 (2) (2016) 1373–1382, <https://doi.org/10.1039/C5SC03727A>.
- [44] W. Wei, Y. Yao, Q.i. Zhao, Z. Xu, Q. Wang, Z. Zhang, Y. Gao, Oxygen defect-induced localized surface plasmon resonance at the WO_{3-x} quantum dot/silver nanowire interface: SERS and photocatalysis, *Nanoscale* 11 (12) (2019) 5535–5547, <https://doi.org/10.1039/C9NR01059A>.
- [45] A.J. Neukirch, W. Nie, J.-C. Blancon, K. Appavoo, H. Tsai, M.Y. Sfeir, C. Katan, L. Pedesseau, J. Even, J.J. Crochet, G. Gupta, A.D. Mohite, S. Tretiak, Polaron stabilization by cooperative lattice distortion and cation rotations in hybrid perovskite materials, *Nano Lett.* 16 (6) (2016) 3809–3816, <https://doi.org/10.1021/acs.nanolett.6b01218>.
- [46] R. Brahimi, K. Dib, M. Trari, Y. Bessekhouad, Effect of S-doping toward the optical properties of WO₃ nanoparticles, *Mater. Chem. Phys.* 223 (2019) 398–403, <https://doi.org/10.1016/j.matchemphys.2018.11.012>.
- [47] K.J. Patel, C.J. Panchal, V.A. Kheraj, M.S. Desai, Growth, structural, electrical and optical properties of the thermally evaporated tungsten trioxide (WO₃) thin films, *Mater. Chem. Phys.* 114 (1) (2009) 475–478, <https://doi.org/10.1016/j.matchemphys.2008.09.071>.
- [48] A. Nakamura, S. Yamada, Fundamental absorption edge of evaporated amorphous WO₃ films, *Appl. Phys.* 24 (1) (1981) 55–59, <https://doi.org/10.1007/BF00900398>.
- [49] H. Cheng, M. Klapproth, A. Sagaltchik, S. Li, A. Thomas, Ordered mesoporous WO_{2.83}: selective reduction synthesis, exceptional localized surface plasmon resonance and enhanced hydrogen evolution reaction activity, *J. Mater. Chem. A* 6 (5) (2018) 2249–2256, <https://doi.org/10.1039/C7TA09579A>.
- [50] B.-R. Koo, K.-H. Kim, H.-J. Ahn, Switching electrochromic performance improvement enabled by highly developed mesopores and oxygen vacancy defects of Fe-doped WO₃ films, *Appl. Surf. Sci.* 453 (2018) 238–244, <https://doi.org/10.1016/j.apsusc.2018.05.094>.
- [51] B.-R. Koo, M.-H. Jo, K.-H. Kim, H.-J. Ahn, Multifunctional electrochromic energy storage devices by chemical cross-linking: impact of a WO₃·H₂O nanoparticle-embedded chitosan thin film on amorphous WO₃ films, *NPG Asia Mater.* 10 (2020) 1–10, <https://doi.org/10.1038/s41427-019-0193-z>.
- [52] Y. Shi, Y. Zhang, K. Tang, J. Cui, X. Shu, Y. Wang, J. Liu, Y. Jiang, H.H. Tan, Y. Wu, Designed growth of WO₃/PEDOT core/shell hybrid nanorod arrays with modulated electrochromic properties, *Chem. Eng. J.* 355 (2019) 942–951, <https://doi.org/10.1016/j.cej.2018.08.163>.
- [53] W. Shen, X. Huo, M. Zhang, M. Guo, Synthesis of oriented core/shell hexagonal tungsten oxide/amorphous titanium dioxide nanorod arrays and its electrochromic-pseudocapacitive properties, *Appl. Surf. Sci.* 515 (2020) 146034, <https://doi.org/10.1016/j.apsusc.2020.146034>.
- [54] J. Pan, R. Zheng, Y.i. Wang, X. Ye, Z. Wan, C. Jia, X. Weng, J. Xie, L. Deng, A high-performance electrochromic device assembled with hexagonal WO₃ and NiO/PB composite nanosheet electrodes towards energy storage smart window, *Sol. Energy Mater. Sol. Cells* 207 (2020) 110337, <https://doi.org/10.1016/j.solmat.2019.110337>.
- [55] P. Cossari, M. Pugliese, C. Simari, A. Mezzi, V. Maiorano, I. Nicotera, G. Gigli, Simplified all-solid-state WO₃ based electrochromic devices on single substrate: toward large area, low voltage, high contrast, and fast switching dynamics, *Adv. Mater. Interfaces* 7 (3) (2020) 1901663, <https://doi.org/10.1002/admi.v7.310.1002/admi.201901663>.
- [56] J.Z. Ou, S. Balendhran, M.R. Field, D.G. Mcculloch, A.S. Zoofakar, R.A. Rani, S. Zhuiykov, A.P. O'mullane, K. Kalantar-zadeh, The anodized crystalline WO₃ nanoporous network with enhanced electrochromic properties, *Nanoscale* 4 (2012) 5980–5988, <https://doi.org/10.1039/C2NR31203D>.
- [57] K. Tang, Y. Zhang, Y. Shi, J. Cui, X. Shu, Y. Wang, Y. Qin, J. Liu, H.H. Tan, Y. Wu, *Electrochim. Acta* 330 (2020), 135189, <https://doi.org/10.1039/C2NR31203D>.
- [58] K. Tang, Y. Zhang, Y. Shi, J. Cui, X. Shu, Y. Wang, Y. Qin, J. Liu, H.H. Tan, Y. Wu, Crystalline WO₃ nanowires array sheathed with sputtered amorphous shells for enhanced electrochromic performance, *Appl. Surf. Sci.* 498 (2019) 143796, <https://doi.org/10.1016/j.apsusc.2019.143796>.
- [59] J. Zhou, Y. Wei, G. Luo, J. Zheng, C. Xu, Electrochromic properties of vertically aligned Ni-doped WO₃ nanostructure films and their application in complementary electrochromic devices, *J. Mater. Chem. C* 4 (8) (2016) 1613–1622, <https://doi.org/10.1039/C5TC03750F>.
- [60] K. Bon-Ryul, K.-H. Kim, H.-J. Ahn, Novel tunneled phosphorus-doped WO₃ films achieved using ignited red phosphorus for stable and fast switching electrochromic performances, *Nanoscale* 11 (7) (2019) 3318–3325, <https://doi.org/10.1039/C8NR08793H>.
- [61] Q. Jiang, N. Kurra, M. Alhabeab, Y. Gogotsi, H.N. Alshareef, All pseudocapacitive MXene-RuO₂ asymmetric supercapacitors, *Adv. Energy Mater.* 8 (13) (2018) 1703043, <https://doi.org/10.1002/aenm.v8.1310.1002/aenm.201703043>.
- [62] E. Lim, C. Jo, M.S. Kim, M.-H. Kim, J. Chun, H. Kim, J. Park, K.C. Roh, K. Kang, S. Yoon, J. Lee, High-performance sodium-ion hybrid supercapacitor based on Nb₂O₅@Carbon core-shell nanoparticles and reduced graphene oxide nanocomposites, *Adv. Funct. Mater.* 26 (21) (2016) 3711–3719, <https://doi.org/10.1002/adfm.v26.2110.1002/adfm.201505548>.
- [63] E. Lim, C. Jo, H. Kim, M.-H. Kim, Y. Mun, J. Chun, Y. Ye, J. Hwang, K.-S. Ha, K. C. Roh, K. Kang, S. Yoon, J. Lee, Facile synthesis of Nb₂O₅@Carbon core-shell nanocrystals with controlled crystalline structure for high-power anodes in hybrid supercapacitors, *ACS Nano* 9 (7) (2015) 7497–7505, <https://doi.org/10.1021/acsnano.5b02601>.